Available online at www.sciencedirect.com
ScienceDirect
Earth and Planetary Science Letters 250 (2006) 581–595
EPSL
www.elsevier.com/locate/epsl

Co-existing fluid and silicate inclusions in mantle diamond

E.L. Tomlinson [a,*], A.P. Jones [b], J.W. Harris [c]

[a] Department of Geology, Royal Holloway University of London, Egham Hill, Egham, Surrey, TW20 0EX, U.K.
[b] Department of Earth Sciences, University College London, Gower Street, London WC1E 6BT, U.K.
[c] Division of Earth Sciences, University of Glasgow, The Gregory Building, Lilybank Gardens, Glasgow, G12 8QQ, U.K.

Received 23 June 2006; received in revised form 1 August 2006; accepted 3 August 2006
Available online 22 September 2006
Editor: R.W. Carlson

Abstract

We document the compositions of co-existing silicate macro-inclusions and fluid micro-inclusions in the fibrous coats of eight coated diamonds from the Panda kimberlite (Canada). The mineral inclusions in the diamond coats come from either the peridotite suite (Cr-pyrope, orthopyroxene, olivine and Cr-diopside) or the eclogite suite (omphacite). Therefore, fibrous diamonds grow in the same paragenetic environments as octahedral diamonds. The inclusions document a more fertile source composition (lower Mg# and higher CaO) than for equivalent phases in octahedral diamonds from Panda and worldwide. However, moderate to high Cr_2O_3 contents in garnet and clinopyroxene inclusions suggest that this apparent fertility is due to a secondary process. Geothermometry of the silicate inclusions yields low equilibration temperatures of 930 to 1010 °C. The co-existing fluid micro-inclusions are dominated by H_2O, carbonate and KCl. Fluid inclusions in both the peridotitic and eclogitic samples fall along linear arrays between Fe–Ca–Mg carbonate and KCl. Inclusions in the one eclogitic sample also contain quartz. We suggest that the diamonds have trapped both metasomatised minerals and the metasomatic fluid, and so provide a snap shot of a metasomatic event in the mantle.

Keywords: coated diamond; silicate inclusions; fluid inclusions; metasomatism

1. Introduction

Fibrous diamonds and the fibrous coats of coated diamonds often contain fluid inclusions trapped along the lateral surfaces of the diamond fibres. The fibrous morphology and presence of fluid inclusions is consistent with rapid diamond growth from a fluid. A remainder of this fluid phase is represented by the inclusions, and provides information on the compositions of mantle fluids during diamond growth [1–6]. These diamonds provide the deepest, and the only pristine, examples of upper mantle fluids. Here we report and examine the relationship between the compositions of co-existing fluid micro-inclusions and peridotitic and eclogitic suite mineral inclusions in the fibrous coats of diamonds from the Panda kimberlite (Canada).

The conditions of diamond growth, such as temperature, pressure and host rock chemistry, are generally determined from the chemistries of non-touching silicate inclusions in diamonds, which are unable to re-equilibrate to subsequent changes in chemical and physical conditions. 'Macro' inclusion (sizes of the order of 100 μm) minerals of the peridotitic (olivine, Cr-pyrope, orthopyroxene, diopsidic clinopyroxene, Mg-chromite), eclogitic (pyrope–almandine garnet and omphacitic clinopyroxene, coesite, kyanite, rutile, sanidine) and "superdeep" (majoritic garnet, ferropericlase, stishovite, CaSi and MgSi perovskite) suites

* Corresponding author.
E-mail address: e.tomlinson@gl.rhul.ac.uk (E.L. Tomlinson).

0012-821X/$ - see front matter © 2006 Elsevier B.V. All rights reserved.
doi:10.1016/j.epsl.2006.08.005

constrain the composition of the host mantle. Geothermobarometry of these inclusions indicate that, in the first two cases, they equilibrated at temperatures of 900–1300 °C and at depths of 150–200 km [7,8] in the lithospheric mantle. The sublithospheric diamonds of the third group come from a depth range from 200 to just below the 660-km upper/lower mantle discontinuity [9].

The much smaller fluid 'micro' inclusions (generally <0.5 μm [10]) present in fibrous diamonds from Botswana and the Democratic Republic of the Congo (DRC) contain fluids that vary between carbonatitic, high in Ca, P and CO_2, and silicate, dominated by Si, Al, K and H_2O [1,2]. Additionally these fibrous diamonds contain quartz, apatite, mica and carbonates [1,11–14]. In contrast, fluid in a fibrous diamond coat from the Diavik Mine (Canada) range in composition from Na–K–Cl brine to Na-rich carbonate [6]. The brine end-member is similar to KCl brine described in internally cloudy diamonds from Koffiefontein (South Africa) [4]. Additionally, primary mantle minerals (Cr-diopside, chromite and olivine) were identified as micro-inclusions phases in the Canadian coated diamond [6] and peridotitic and eclogitic silicates and carbonates were detected as a component of the micro-inclusions in cloudy diamonds from Koffiefontein [5]. However, single phase mineral inclusions have not previously been described from fibrous diamonds.

2. Geological setting, previous work and samples

Panda is a group I (basaltic) kimberlite that intruded the Central Slave Craton 52.3±3.8 Ma ago [15]. The xenocryst population of the Panda kimberlite consists of mantle-derived olivine, garnet, pyroxene (Cr-diopside and enstatite), chromite and ilmenite [16]. The lithosphere below the Slave Craton consists of two distinct compositional layers [17,18]: an ultra-depleted harzburgite-dominated upper layer that straddles the diamond–graphite boundary at 4.2 GPa, 900 °C [17], and a deeper layer dominated by more fertile lherzolite.

Silicate mineral inclusions in octahedral diamonds from Panda are dominantly peridotitic (≈85%) [19] and equilibrated at 1100–1250 °C [20]. Westerlund et al., [21] derived an age of 3408±280 Ma for peridotitic octahedral diamonds from this kimberlite by Re–Os dating of sulphide inclusions. Eclogitic diamond inclusions include jadeite-poor clinopyroxene and garnet and have not yet been dated. A distinctive feature of the Panda diamond production is the high proportion of coated diamonds, this probably reflects low degrees of diamond resorption during kimberlite ascent [20].

For this study, eight milky grey to black, coated diamonds (fibrous diamond 'coat' on an octahedral diamond 'core') from Panda (0.17–0.29 ct) were made into doubly polished wafers with [100] orientation. Cathodoluminescence images of all the samples show that the coats are composed of a single growth zone. Prior to analysis, all the samples were cleaned using HCl, acetone and then distilled water. The sample characteristics are summarised in Table 1.

3. Analytical method

3.1. FT-IR

Infrared absorption spectra were collected using a Vector22 Fourier Transform infrared (FTIR) spectrometer equipped with a HeNe laser (633 nm), a KBr beam splitter, a 5× beam condenser and a deuterated triglycine sulfate (DTGS) detector. The beam diameter was approximately 0.6 mm. Spectra were recorded in

Table 1
Summary of Panda diamond coat characteristics determined from FTIR spectroscopy and EMPA

Sample	Core		Coat						
	N	%B	Suite	N	H_2O	H_2O#	Minerals present	T (°C)	P (Gpa)
PAN1	–	–	P	580	61	68	Olivine^{x,y,z}, cpx^{z}, carb.^{x}		
PAN2	500	33	P	405	33	64	Olivine^{z}, carb.^{x}		
PAN3	–	–	P	1345	351	63	Pyroxene^{x}, (cpx^{y}, opx^{y}), carb.^{x}	935^{c}	4.2^{c}
PAN4	–	–	E	1560	354	68	Cpx^{x,y,z}, rutile^{y}, quartz^{x}, carb.^{x}		
PAN5	585	30	P	1270	564	59	Garnet^{x,y}, cpx^{y,z}, carb.^{x}	959^{b}, 980^{c}	4.6^{c}
PAN6	1040	10	P	600	31	56	Olivine^{z}, carb.^{x}		
PAN7	1550	8	P	1660	248	55	Olivine^{y}, carb.^{x}		
PAN8	1200	3	P	845	251	56	Garnet^{y}, olivine^{y}, carb.^{x}	1006^{a}	

Nitrogen aggregation state quoted as percentage of IaB aggregate in the diamond core. Nitrogen and H_2O concentrations are given in ppm. $H_2O\# = 100H_2O/(H_2O+CO_2)$. Mineral phases as detected in: ^{x}FTIR absorption spectra, EMPA as ^{y}single phase macro-inclusions or ^{z}micro-inclusion phases. Pressure and temperature conditions are calculated from macro-inclusion compositions using the geothermometers in ^{a}[28,32], ^{b}[33] and the geothermobarometer in ^{c}[34]. Garnet–olivine temperatures were calculated for an assumed pressure of 4.6 GPa.

transmission with a resolution of 2 cm^{-1} in the range 4000 to 380 cm^{-1} with one spectrum being the average obtained from 512 scans. An Al foil mask was used to ensure that only the fibrous coat was analysed. Lattice-bound nitrogen concentrations are determined using the method of Mendelssohn and Milledge [22] (Table 1).

Nitrogen is present as mildly aggregated IaA in all of the diamond coats, this is consistent with global fibrous diamond populations [23–25]. Nitrogen concentrations range between 403 and 1660 ppm in the coats. Lattice bound nitrogen in the Panda diamond cores is more aggregated than in their coats, having up to 33% IaB centres with some platelet development and nitrogen concentrations of 500 to 1540 ppm.

The concentrations of H_2O and carbonate as CO_2 were calculated from the intensities of the O–H stretching band of water (using ε_{3420}=80 L/mol cm^{-1}, [26]) and of the ν_3 stretching band of calcium carbonate (using ε_{1430}=235 L/mol cm^{-1}, [27]). Taking into account the difference in absorption coefficients of different carbonates and the effect of pressure on water and carbonate absorption, the error on the calculated H_2O and CO_2 concentrations are estimated as ±25 and ±40 ppm, respectively [1]. Since the absolute concentration of volatiles is dependent on inclusion density, we use the ratio $H_2O\#=H_2O/(CO_2+H_2O)$ to describe the volatile composition.

3.2. Electron microprobe analyses

Electron Microprobe Analyses (EMPA) of individual macro- and micro-inclusions in the diamond coats were performed using a JEOL Superprobe 733. Analyses were carried out using an accelerating voltage of 15 keV and a beam current of 10 nA, at these conditions the spot diameter was approximately 2 μm. The instrument is equipped with an Energy Dispersive Spectrometer (EDS), a collimator and a SiLi crystal detector with an atmospheric thin window (ATW). The channel width is 0.01 KeV and the resolution (the full width half maximum of Mn) is 138 eV. The count rate was 6 to 7 kcps for a count time of 100 s. Spectra were reduced using the Oxford Instruments Link ISIS SEM-Quant (ZAF) correction relative to a cobalt standard.

3.2.1. Macro-inclusions

Silicate inclusions were exposed during polishing of six of the eight Panda coated diamonds. Both peridotitic (PAN1, PAN3, PAN5, PAN7, PAN8) and eclogitic parageneses (PAN4) are represented. Silicate inclusions in the coated diamonds are small (typically 2 to 20 μm) and abundant. Inclusions at the small end of the size range do not give 100% totals. Table 2 shows the average compositions of each phase in each sample, the full data set is available as online supplementary material. Multiple analyses (20) of a single clinopyroxene grain in PAN4 revealed good reproducibility, with the following standard deviations in wt.% (1σ): SiO_2 (0.22), Al_2O_3 (0.09), FeO (0.10), Cr_2O_3 (0.08), MgO (0.08), CaO (0.09), TiO_2 (0.12).

Inclusions in the Panda diamond coats are compared to inclusions in octahedral Panda diamonds analysed by WDS. Only differences in the major element concentrations (Mg, Fe, and Ca) are considered, because of the lower resolution of the EDS. Errors for Mg# (=Mg/(Mg+Fe))

Table 2
EMPA analyses of silicate inclusions in diamond coats from Panda

Sample	PAN8		PAN5		PAN1	PAN3		PAN7	PAN4
Phase	Garnet	Olivine	Garnet	Cpx	Olivine	Cpx	Opx	Olivine	Cpx
Paragenesis	Lherz.	Lherz.	Lherz.	Lherz.	Lherz.	Lherz.	Lherz.		Ecl.
SiO_2	41.6	44.2	42.3	55.6	44.0	55.8	64.4	43.9	55.6
TiO_2	0.2	nd	nd	nd	nd	0.3	nd	nd	nd
Al_2O_3	17.0	0.2	17.9	1.1	nd	1.7	1.1	nd	7.2
Cr_2O_3	8.4	nd	7.6	1.8	nd	2.2	nd	0.1	nd
FeO	7.2	7.8	6.7	1.8	8.4	1.9	5.0	7.3	6.9
NiO	0.2	0.4	0.2	nd	0.3	nd	0.3	0.5	0.4
MgO	18.1	47.0	17.7	17.2	47.0	16.1	28.3	47.9	9.8
CaO	5.4	0.1	6.4	21.5	0.2	20.1	0.3	nd	15.7
Na_2O	0.3	0.2	0.2	1.1	0.3	1.5	0.2	0.3	4.7
K_2O	0.5	nd	0.2	nd	nd	0.2	0.2	nd	nd
Mg#	81.7	91.4	82.6	94.6	90.9	93.7	91.0	92.1	71.8
Ca#	14.8	–	17.6	45.8	–	45.7	0.6	–	45.1

Average compositions of each phase are given, the full data set is available in the online supplementary materials. Totals are normalised to 100 wt.% and the analysed total is given, the analysed totals are also given. Cations are calculated on the basis of 6 (olivine clinopyroxene, orthopyroxene) and 24 (garnet) oxygens. Mg#=100Mg/(Mg+Fe), Ca#=100Ca/(Ca+Mg+Fe). Abbreviations: Lherz. — lherzolite, Ecl .— eclogite, nd — not detected.

Table 3
Compositions of fluid inclusions in coated diamonds from Panda

Sample	PAN2			PAN3			PAN5			PAN6		
Inc. no.	18	41	Ave. (σ)	2	12	Ave. (σ)	25	28	Ave. (σ)	1	10	Ave. (σ)
wt.% oxide												
SiO_2	3.9	3.8	4.6 (2.2)	4.6	2.8	3.1 (0.7)	7.8	8.1	5.8 (2.5)	5.6	3.3	4.0 (2.2)
TiO_2												
Al_2O_3	1.3	0.9	1.4 (1.4)		0.7	0.8 (0.6)		1.1	1.9 (1.9)			1.3 (0.4)
MgO	14.9	2.1	5.7 (3.9)	6.0	2.8	3.3 (1.6)	6.4	10.8	7.8 (5.6)	11.3	2.9	4.6 (3.4)
FeO	29.4	5.4	12.2 (7.8)	12.6	6.3	6.9 (2.5)	23.4	29.6	26.8 (14.2)	36.5	16.0	16.9 (11.4)
CaO	19.9	2.6	7.1 (4.8)	7.7	3.6	4.9 (2.3)	8.4	14.0	12.7 (9.6)	16.4	8.7	7.6 (4.9)
BaO	6.3	11.2	12.0 (6.7)	17.6	16.6	17.2 (4.7)	7.3	16.4	11.4 (7.3)	21.8	11.6	15.7 (4.7)
Na_2O	2.2	4.4	3.9 (1.7)	4.9	4.9	4.6 (0.9)	2.9	3.2	5.9 (4.4)	2.5	4.1	7.6 (3.4)
K_2O	10.2	34.3	22.4 (10.7)	23.0	31.0	27.9 (5.9)	21.1	5.4	12.7 (10.8)	1.4	28.9	21.9 (11.3)
P_2O_5												
Cl	7.5	32.8	21.3 (9.3)	23.6	29.6	29.2 (4.3)	19.6	4.7	13.1 (10.9)	1.9	24.6	23.4 (9.6)
Total	21.2	12.8	13.5 (4.9)	6.5	6.3	6.1 (2.3)	6.6	8.3	7.9 (1.9)	9.7	10.0	7.9 (3.6)
mol. %												
Si	4.0	3.8	5.0 (4.7)	4.7	2.9	3.2 (3.2)	7.9	9.5	6.1 (3.8)	6.5	3.3	4.0 (4.2)
Ti												
Al	0.8	0.5	0.9 (1.7)		0.4	0.5 (1.5)		0.8	1.2 (1.7)		0.0	0.8 (0.5)
Mg	23.0	3.1	9.1 (12.3)	9.1	4.3	4.9 (10.8)	9.7	18.8	12.3 (12.6)	19.7	4.4	6.8 (10.1)
Fe	25.4	4.5	11.0 (13.7)	10.7	5.4	5.9 (9.7)	19.9	28.9	23.6 (17.8)	35.7	13.5	14.0 (18.7)
Ca	22.1	2.8	8.2 (10.8)	8.4	3.9	5.3 (11.3)	9.2	17.5	14.3 (15.4)	20.5	9.4	8.1 (10.3)
Ba	2.6	4.3	7.3 (5.5)	7.0	6.7	6.9 (8.4)	2.9	7.5	4.7 (4.3)	10.0	4.6	6.1 (3.6)
Na	2.2	4.2	4.1 (3.6)	4.8	4.9	4.6 (4.0)	2.9	3.6	6.0 (6.4)	2.8	4.0	7.3 (6.4)
K	6.7	21.7	15.4 (14.4)	14.9	20.2	18.2 (17.2)	13.7	4.0	8.5 (10.3)	1.0	18.6	13.8 (14.2)
P												
Cl	13.2	55.1	38.9 (33.3)	40.6	51.4	50.5 (33.9)	33.8	9.3	23.3 (27.7)	3.8	42.1	39.2 (32.0)
K/Cl	0.51	0.39	0.40 (0.43)	0.37	0.39	0.36 (0.51)	0.40	0.43	0.37 (0.37)	0.28	0.44	0.35 (0.44)
KNa/Cl	0.68	0.47	0.50 (0.54)	0.49	0.49	0.45 (0.63)	0.49	0.82	0.62 (0.60)	1.03	0.54	0.54 (0.64)
CaFeMg/Cl	5.36	0.19	0.73 (1.11)	0.69	0.26	0.32 (0.94)	1.15	7.01	2.15 (1.65)	20.3	0.65	0.74 (1.22)
Ca/(CaMgFe)	0.31	0.27	0.29 (0.29)	0.30	0.29	0.33 (0.36)	0.24	0.27	0.29 (0.34)	0.27	0.34	0.28 (0.26)

The average composition and standard deviation are given for each sample, in addition to two representative inclusion compositions. The total molecular proportions and the total oxide plus chlorine contents are normalised to 100 wt.%, with the analysed total also given. The calculated brine and carbonate end-members for the peridotite and eclogite suite inclusions are also given. The full data set can be found in the online supplementary materials.

and Ca# (=Ca/(Ca+Mg+Fe)) of each silicate inclusion are derived by propagating an error of 3σ, the quoted value is the worst example of each phase.

3.2.2. Micro-inclusions

Individual inclusions were identified immediately below (<1 μm) the surface of the diamond coats using backscattered electron imaging mode. The inclusions are completely enclosed in the diamond host and are not connected to the diamond surface by cracks. Because of the low mean atomic number of diamond, the electron beam shows a significant degree of penetration into the sample with an activation volume of approximately 4 μm^3 at 15 KeV, this is larger than the average inclusion volume (<1 μm^3).

The small size and high volatile contents of the inclusions means that analysed totals are significantly lower than 100%, the average oxide plus chlorine concentration is 12 wt.% (2 to 45 wt.%). The sum of oxides plus chlorine was normalised to 100 wt.% (with excess oxygen for Cl) in order to remove the effect of variable inclusion size, depth and C–O–H content. Normalising the data to 100% assumes a uniform distribution of carbon and oxides in the analysed volume. In actual fact, the inclusions consist of oxides surrounded by carbon matrix, therefore low energy X-rays from light elements will be more strongly attenuated. Navon, cited in [5] calculated that this has a small effect on most of the analysed elements, but is ~ 10% (relative) for Na, and higher for lighter elements. The accuracy of the analyses of oxides for single inclusions is approximately 10–20% (relative), on the basis of repeated analysis of olivine and clinopyroxene detected in micro-inclusions.

The following elements were analysed in the micro-inclusions (brackets show the detection limits at 95%

PAN7			PAN8			PAN4			Peridotitic		Eclogitic	
2	30	Ave. (σ)	10	13	Ave. (σ)	14	20	Ave. (σ)	Brine (±)	Carb. (±)	Brine (±)	Carb. (±)
7.6	2.7	3.5 (1.4)	2.8	4.5	4.5 (2.1)	25.9	12.3	15.1 (6.4)	2.2 (0.5)	7.6 (0.4)	3.4 (3.4)	39.1 (4.6)
			5.5	9.8	6.1 (2.5)			0.3 (0.6)	–	–	–	–
	0.9	0.8 (0.1)				2.8	1.1	1.7 (0.7)	–	2.5 (1.1)	0.7 (0.1)	4.0 (0.2)
11.0	3.0	4.9 (3.1)	2.8	6.6	5.5 (4.2)	1.8	0.9	1.2 (1.0)	0.0 (0.7)	14.1 (2.6)	0.0 (0.0)	4.3 (0.0)
31.7	19.6	18.9 (13.8)	5.5	19.3	13.6 (11.3)	11.1	8.2	9.8 (3.3)	1.4 (2.0)	37.6 (0.7)	9.4 (0.4)	12.8 (0.4)
15.6	5.8	9.0 (5.6)	3.6	8.8	7.4 (6.2)	5.8	3.5	4.9 (1.8)	0.7 (0.7)	19.9 (1.7)	0.6 (0.2)	12.7 (0.3)
17.6	9.9	12.0 (7.1)	5.6	12.1	11.9 (5.2)	11.3	11.9	13.2 (3.4)	14.7 (5.3)	16.6 (1.7)	11.2 (2.1)	14.3 (2.8)
4.0	6.7	9.0 (5.3)	13.4	4.5	11.8 (5.5)	3.0	4.5	4.1 (0.8)	10.3 (4.2)	1.6 (0.5)	3.6 (0.1)	5.0 (0.1)
4.3	26.2	19.9 9.2)	30.0	22.7	22.4 (9.1)	22.3	30.3	26.0 (6.9)	34.3 (0.5)	–	37.4 (2.8)	0.0 (4.2)
						2.3	2.2	2.6 (1.3)	–	–	1.2 (0.5)	7.9 (1.5)
4.2	23.6	21.4 (9.6)	34.6	21.1	26.6 (11.2)	14.0	25.2	22.2 (6.6)	36.5 (11.9)	–	32.5 (0.4)	0.0 (0.0)
7.8	29.3	23.2 (10.1)	5.1	6.7	5.1 (1.4)	4.3	6.9	8.0 (3.8)	–	–	–	–
8.6	2.8	3.5 (2.6)	2.5	4.2	4.0 (3.6)	28.1	12.7	15.7 (20.1)	2.1 (0.3)	8.4 (0.7)	3.4 (3.4)	45.8 (4.4)
			3.7	6.9	4.1 (3.2)			0.2 (1.5)	–	–	–	–
	0.5	0.5 (0.2)				1.8	0.7	1.0 (1.3)	–	1.6 (0.8)	0.4 (0.0)	2.7 (0.1)
18.7	4.6	7.3 (8.7)	3.8	9.2	7.3 (10.7)	2.9	1.4	1.9 (4.7)	0.0 (1.5)	23.1 (3.6)	0.0 (0.0)	7.4 (0.2)
30.2	16.8	16.0 (21.5)	4.1	15.1	10.2 (16.2)	10.1	7.1	8.5 (8.7)	1.1 (2.9)	34.6 (1.8)	7.9 (1.5)	12.5 (0.1)
19.0	6.4	9.7 (11.2)	3.5	8.9	7.1 (11.3)	6.8	3.9	5.5 (5.9)	0.7 (1.4)	23.4 (1.3)	0.7 (0.1)	16.0 (0.0)
7.9	4.0	4.8 (5.2)	1.9	4.4	4.2 (3.5)	4.8	4.8	5.4 (4.2)	5.6 (5.6)	7.2 (1.0)	4.4 (2.1)	6.6 (1.5)
4.4	6.7	8.8 (9.6)	11.5	4.1	10.2 (9.1)	3.2	4.5	4.1 (2.6)	9.6 (10.3)	1.7 (0.6)	3.5 (1.0)	5.7 (0.3)
3.1	17.2	12.8 (10.9)	17.0	13.6	12.8 (9.9)	15.5	19.9	17.3 (13.9)	21.1 (9.5)	–	24.0 (8.0)	0.0 (3.2)
						1.1	1.0	1.1 (1.7)	–	–	0.4 (0.1)	3.2 (0.5)
8.1	41.1	36.6 (30.2)	52.1	33.6	40.3 (32.5)	25.8	44.1	39.2 (35.2)	59.7 (0.3)	–	55.4 (12.6)	0.0 (0.0)
0.39	0.42	0.35 (0.36)	0.33	0.40	0.32 (0.31)	0.60	0.45	0.44 (0.40)	–	–		
0.93	0.58	0.59 (0.68)	0.55	0.53	0.57 (0.58)	0.72	0.55	0.55 (0.47)	–	–		
8.37	0.68	0.90 (1.37)	0.22	0.99	0.61 (1.17)	0.77	0.28	0.41 (0.55)	–	–		
0.28	0.23	0.29 (0.27)	0.31	0.27	0.29 (0.30)	0.34	0.31	0.35 (0.31)	–	–		

confidence): Si (0.05%), Ti (0.13%), Al (0.06%), Mg (0.07%), Fe (0.15%), Ca (0.08%), P (0.08%), Na (0.08%), K (0.09%) and Cl (0.09%). The mean of the individual inclusion compositions measured in a sample was taken to represent the bulk major element composition of that sample. The bulk and two representative individual inclusion analyses for each sample are given in Table 3; the full data set is available as online supplementary material.

4. Results

4.1. Macro-inclusions

Olivine, garnet and pyroxene were identified in the infrared spectra of the diamond coats (Fig. 1) and from EMPA (Table 1). No silicate inclusions were observed in the diamond cores.

4.1.1. Garnet

Two diamond coats contain garnet inclusions (PAN8 and PAN5). The garnets have moderate Cr_2O_3 (7.3 to 8.9 wt.%) and high CaO contents (5.1 to 6.7 wt.%) and are classified as lherzolitic Cr-pyrope (Fig. 2). The chemistry of these garnet inclusions overlap with the compositions of garnet inclusions in octahedral diamonds from Panda [19,20] and extend the range to more Ca- and Fe-rich compositions.

The Mg# of the garnets varies between 80.6 and 84.3 with an average of 82.0 (±1.2). The effect of Ca on the Mg–Fe partitioning between garnet and olivine was eliminated by recalculating all garnets to a Ca-free composition according to the method in [20]. From the data in [28], it can be estimated that the Mg# of garnet decreases by 2.0 per cation Ca ([O] =24) at 1000 to 1100 °C and 5 GPa, when coexisting with olivine with an Mg# of 91. The recalculated

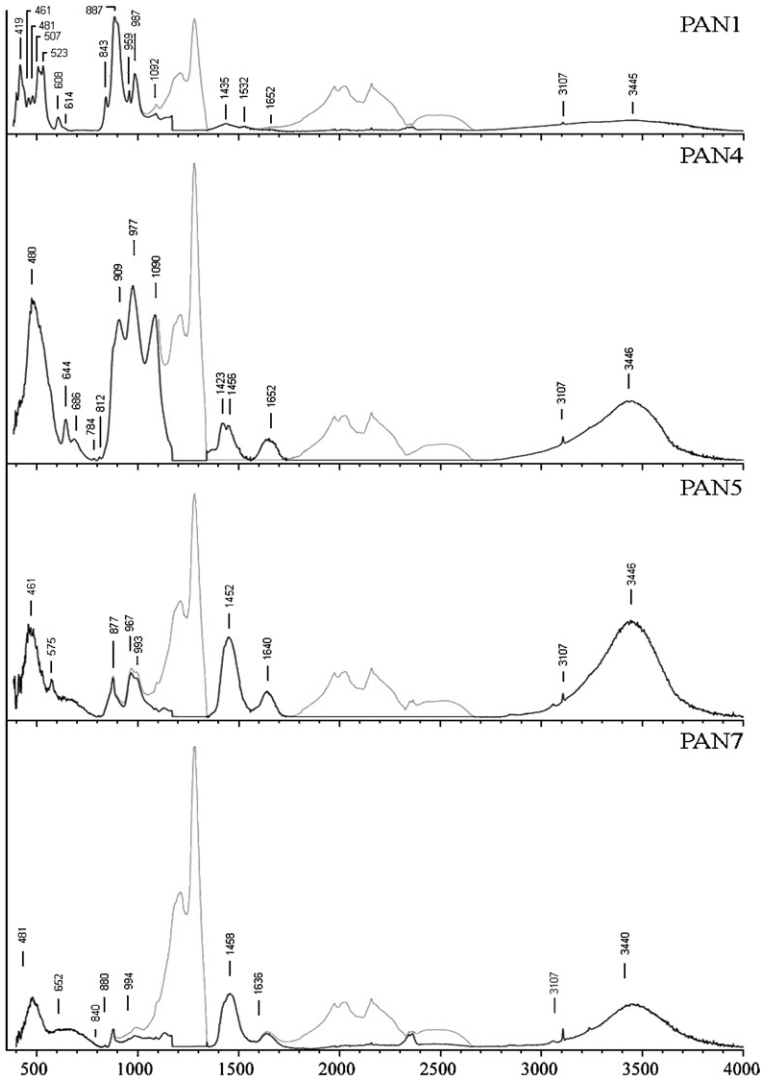

Fig. 1. Infrared absorption spectra of selected Panda diamond coats. The original spectra shown by the grey line, the black line shows the result after subtraction of the residual IaA diamond spectrum. All spectra show a wide absorption band at $\approx 3440\ cm^{-1}$ and the band at $\approx 1652\ cm^{-1}$ is due to the presence of OH. Minerals present include: olivine (PAN1: 887, 507, 987, 608, 532 and 843 cm^{-1}), pyroxene (PAN4: 1090, 480, 877 (shoulder), 520, 977, 908, 644 cm^{-1}), garnet (PAN5: 484, 877, 904 (shoulder), 575, 967, 993 cm^{-1}), quartz (PAN4: 812 and 784 cm^{-1}) and carbonate (880 and 1460–1420 cm^{-1}). Additionally, all samples have a sharp peak at 3107 cm^{-1} due to lattice bound hydrogen.

Mg#'s of the Panda garnets vary between 82.4 and 86.1 (mean = 83.8); the mean Mg# for Slave Cr-pyrope inclusions in diamond is 87.0 and for worldwide samples 87.9 [20]. Therefore, the garnet Mg# values are low.

Low Mg# values are generally considered to be indicative of a high source fertility (i.e. not significantly affected by depletion through partial melting) and low equilibration temperatures. However the Cr-content of the Panda coat inclusions is not consistent with high fertility. The garnet inclusions also have high Na_2O concentrations (0.2 to 0.40 wt.%), a characteristic shared by garnets in octahedral diamonds from Panda [19]. In all the garnets, the TiO_2 concentrations are below the 0.4 wt.% cut-off value used as an indicator of metasomatism by silicate melts [29,30].

4.1.2. Olivine

Three of the coated diamonds contain olivine inclusions (PAN1, PAN7 and PAN8). The olivines have forsterite contents of Mg# = 89.7 to 93.1 (±0.6);

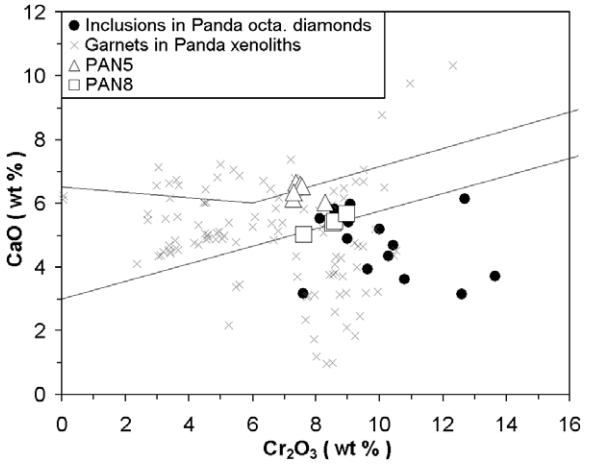

Fig. 2. Cr_2O_3 verses CaO for garnet inclusions in diamond coats PAN5 (large open triangles) and PAN8 (large open squares). Also shown are compositions of garnet inclusions in octahedral (octa.) diamonds from Panda, data from [19,20] (small closed circles) and of garnets from Panda peridotite xenoliths from [17] (small diamonds).

this is within the lower half of the worldwide database for inclusions in diamonds and extends the range recorded in olivine inclusions in octahedral Panda diamonds (91.9–93.2 [19,20]) to lower Mg numbers. In consequence, there is an overlap between the Mg# values of olivine inclusions in the Panda diamond coats and olivine xenocrysts from the Panda kimberlite (generally 90–93, [17]). NiO concentrations range from 0.3 to 0.5 wt.% and are within the range of NiO content of inclusions in octahedral diamond from Panda (0.19 to 0.40 wt.%, [19]) and worldwide [19].

4.1.3. Clinopyroxene

Eclogitic (PAN4) and peridotitic (PAN3, PAN5 and PAN8) clinopyroxenes are represented in the Panda coated diamond inclusion population. Eclogitic clinopyroxene inclusions are found in sample PAN4 and have molar ratios of Mg#=70.1 to 72.9 and Ca#=to 44.5 to 45.9 and so are omphacitic. Al_2O_3 and Na_2O concentrations are low (7.1±0.3 wt.% and 4.7±0.2 wt.%, respectively) relative to eclogitic clinopyroxene inclusions from Snap Lake and from worldwide sources. Cr_2O_3 concentrations are generally at or below the detection limit (0.08 wt.%).

Peridotitic clinopyroxenes have molar ratios of Mg#=92.8 to 95.0 (±1.8) and Ca#=43.8 to 46.7 (±1.5); they have Cr_2O_3 concentrations of 1.2 to 2.9 wt.% and so are Cr-diopsides. These compositions are less magnesian and more Ca-rich than the world average and overlap both with those of clinopyroxene inclusions in

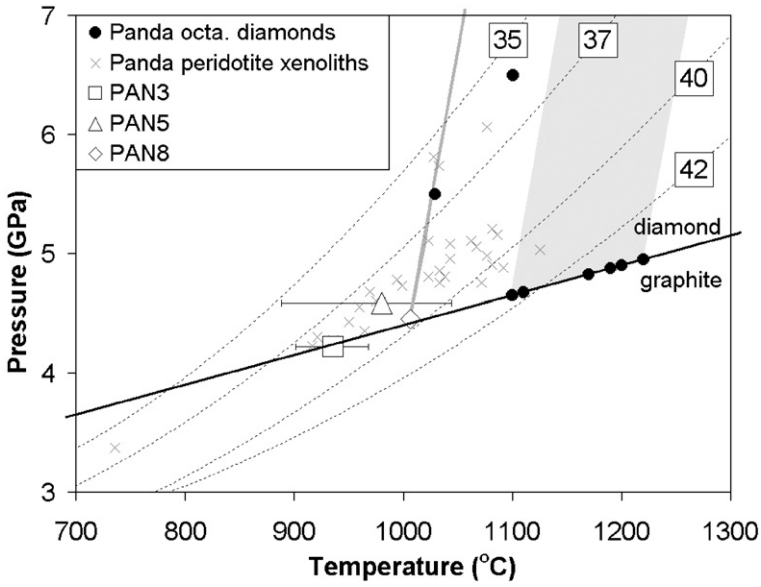

Fig. 3. Average pressure–temperature conditions of clinopyroxene equilibration in samples PAN3 and PAN5 calculated using [34] (error bars show the range of conditions calculated using the full range of compositions), and the temperature of PAN8 calculated for a range of pressures (dark grey line) calculated using the garnet–olivine geothermometer from [28,32]. Black circles are the temperatures of formation of non-touching pairs of garnet–olivine inclusions in octahedral (octa.) diamonds from Panda calculated at 5 GPa; the light shaded area represents the range of temperatures at given pressures of inclusions in octahedral diamonds [19] and of clinopyroxene crystals in mantle xenoliths (small solid black circles) from Panda (open diamonds) [17] calculated using [34]. Dashed lines show conductive geotherms (in mW/m^2) for various surface heat flow values calculated after [35], the graphite–diamond stability boundary [50] is shown as a solid black line.

octahedral diamonds [19] and clinopyroxene inclusions in xenoliths from Panda [17] (Mg# of 91 to 93). This suggests a high source fertility, however the inclusions also have moderate Cr# (=100Cr/(Cr+Al)) of 27.2 to 55.2, compared to clinopyroxene inclusions in xenoliths from Panda (Cr# of 22.8 to 52.7 [17]).

The Cr-diopside inclusions have Al_2O_3 contents of 0.8 to 2.5 wt.% and Na_2O concentrations of 0.7 to 2.3 wt.%. Clinopyroxene inclusions in sample PAN3 are compositionally heterogeneous, showing a range of CaO, Al_2O_3, FeO, MgO and Na_2O contents. K_2O concentrations in clinopyroxene inclusions are generally below the detection limit, and coexist with KCl-bearing fluid micro-inclusions in the Panda diamond coats. This may suggest the local presence of a K-rich phase, such as phlogopite [31], however phlogopite was not detected in any of the samples in this study. Alternatively, KCl may coexist with K-poor clinopyroxene if the partition coefficient, $K^{cpx/KCl}$, is significantly less than one.

4.1.4. Orthopyroxene

Four orthopyroxene inclusions were analysed, all from PAN3. Like the Cr-pyrope and olivine inclusions, orthopyroxenes have relatively low Mg# values of 89.8 to 92.2 (±1.4).

4.1.5. Inclusion geothermobarometry

We have estimated the temperature of fibrous diamond growth using the non-touching inclusion assemblages in peridotitic samples PAN8 (garnet–olivine, [28,32]); PAN5 (garnet–clinopyroxene, [33]); PAN3 and PAN5 (enstatite-in-clinopyroxene, [34]). Pressure was estimated using the Cr-in-clinopyroxene barometer of [34] in samples PAN3 and PAN5.

Geothermobarometry indicates that the peridotitic diamond coats grew at an average temperature of 930–1010±50 °C and pressures of 4.2 to 4.6 GPa (Table 1, Fig. 3). These conditions are right on the diamond stability line, and overlap with pressure–temperature estimates from xenocrysts in the Panda kimberlite. This low temperature may account for the low degree of nitrogen aggregation. These temperatures are slightly lower than those calculated for non-touching pairs of inclusions in non-fibrous diamonds from Panda (1061 to 1233 °C, [19]). The calculated *PT* conditions place the Panda coats on a geotherm of 37 to 40 mW/m^2 [35], this is slightly lower than for world-wide diamond sources, where geothermal gradients of about 40–42 mW/m^2 have been deduced [36–38]. The geothermal gradient of the diamond coats are similar to the geothermal gradient indicated by touching garnet and orthopyroxene pairs in Panda octahedral diamonds [19,20], which have re-equilibrated to the lower temperatures after entrapment in the diamond. The calculated equilibration temperatures are below the lherzolite–H_2O–CO_2 solidus of Wyllie [39].

Compositional disequilibrium in PAN8 leads to wide variations in temperature: calculated temperatures

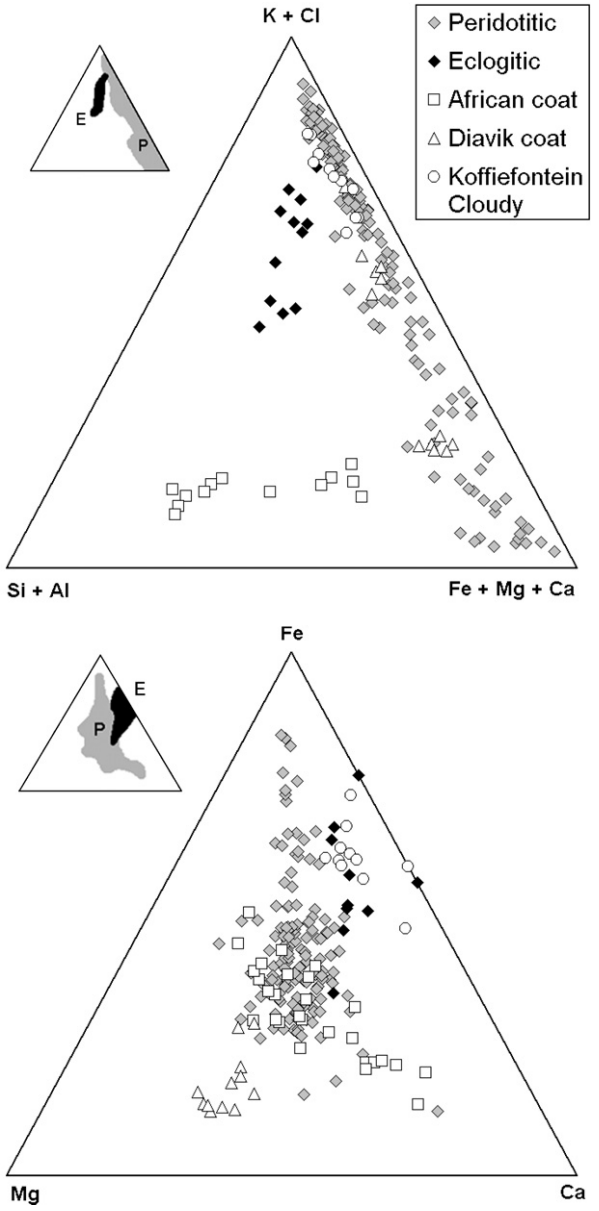

Fig. 4. Compositions of micro-inclusions in peridotitic (grey diamonds; PAN1, PAN2, PAN3, PAN5, PAN6, PAN7, PAN8) and eclogitic (black diamonds; PAN4) coated diamonds from Panda. Also shown are published data from coated diamonds from Africa [1,2] (open squares) and Diavik (Canada) [6] (open triangles) and cloudy diamonds from Koffiefontein [4] (open circles). Summary insets show the compositional fields of inclusions in the peridotitic (P, grey) and eclogite (E, black) samples.

ranging from 730 to 1090 °C depending whether low-Mg or high-Mg garnet–olivine pairs were used. The maximum temperature variation calculated within the other samples is <100 °C. This wide range calculated temperature in PAN8 is unlikely to be the true temperature range because it is not recorded in the other samples, more likely this reflects varying degrees of disequilibrium between coexisting minerals.

4.2. Micro-inclusions

Carbonate and water are present in the infrared spectra of all the Panda diamond coats (Fig. 1). The inclusion spectra are dominated by an intense O–H stretching band in the 2800–3800 cm^{-1} region, due to the presence of hydrogen-bonded O-containing species in the inclusions. The species are identified as molecular H_2O by the strong H_2O ν_2 bending vibration at 1656 cm^{-1} (Fig. 1). The ratio $H_2O\#$ ($100H_2O/(CO_2+H_2O)$) is ≈61 (58 to 70). The broad band centred at 1447 cm^{-1} in both the peridotitic and eclogitic samples is due to the asymmetric stretching vibration (ν_3) of CO_3^{2-} groups [40], whilst the eclogitic sample (PAN4) has a second carbonate peak centred at 1423 cm^{-1} suggesting the presence of a second carbonate species. Quartz is only observed in the single eclogitic sample.

The samples contain Fe–Ca–Mg carbonates, K–Na–Cl brine and silicates; no sulphides are detected. The inclusions span a wide compositional range and the samples are not zoned in terms of major elements. In addition to their occurrence as macro-inclusions, olivine (PAN1, PAN2, PAN3, PAN6) and clinopyroxene (PAN1,

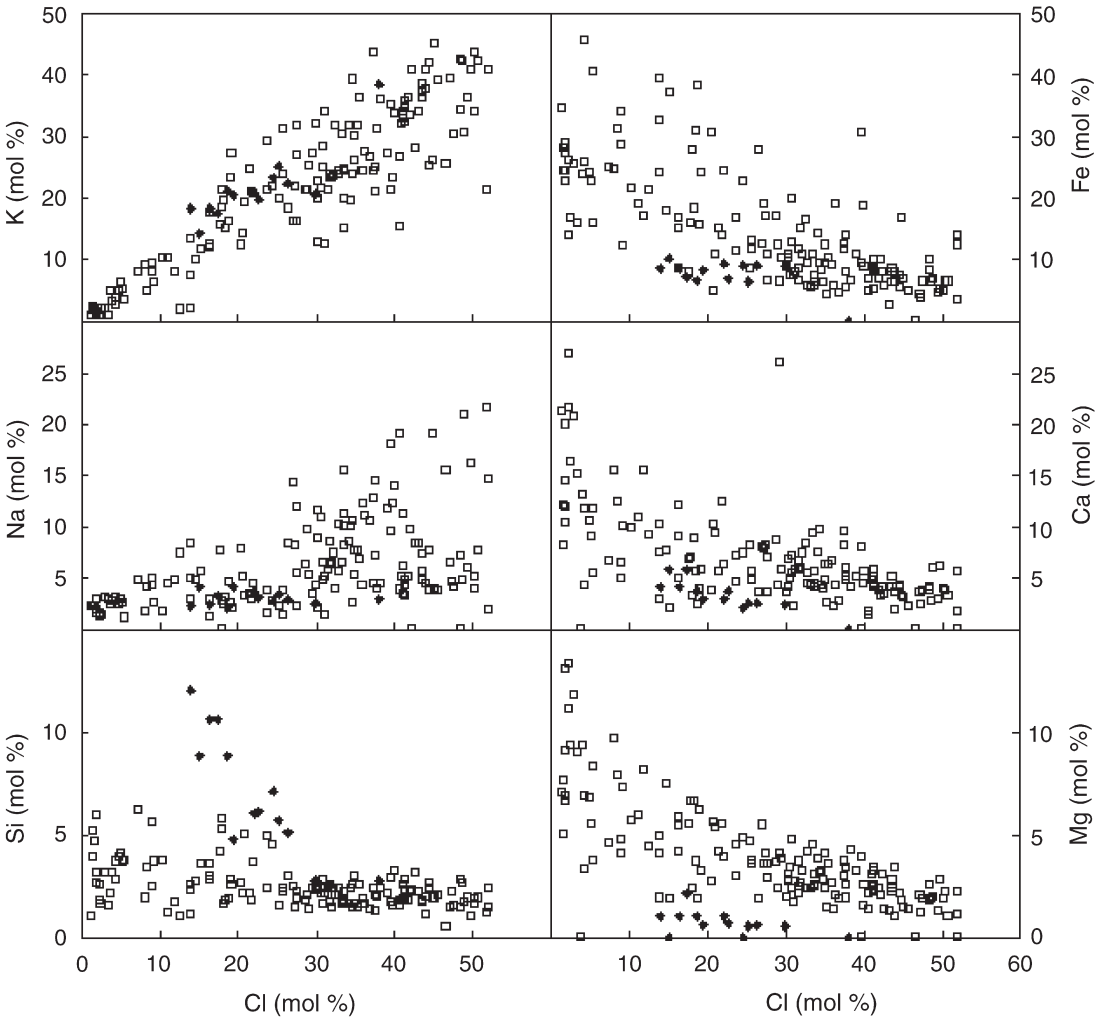

Fig. 5. Variation diagrams showing the 100% normalized molecular proportions of various elements in relation to Cl in the peridotitic (open squares) and eclogitic (blank diamonds) Panda diamond coat fluids.

PAN4, PAN5) are present in the micro-inclusions, where they coexist with K–Na–Cl fluid and/or carbonate. The compositions of these mineral phases are poorly constrained as they are present in very small, multi-phase inclusions. Peridotitic and eclogitic inclusions do not occur mutually within samples. Micro-inclusions containing these mantle silicates are not considered in the following sections detailing the compositions of the coexisting brine and carbonate fluid in the peridotitic and eclogitic samples.

4.2.1. Peridotitic

Micro-inclusion compositions in the peridotitic coated diamonds from Panda contrast with inclusions in African [1,2] samples which have higher concentrations of SiO_2 and Al_2O_3. The inclusions are similar to inclusion compositions described in a single fibrous diamond from Diavik [6] (Fig. 4). Fe, Mg and Ca are present in all Panda inclusions and often in the absence of Si and Al. This observation, combined with the presence of carbonate bands in the FTIR spectra of all samples, indicates that the micro-inclusions contain carbonate. The average Mg# is 0.42±0.1. The peridotitic diamond coat fluids also have high concentrations of Ba (5–8 mol%).

The chemistry of the micro-inclusions in the peridotitic diamonds shows that Cl is negatively correlated with Ca, Mg, Fe and Si and positively correlated with K and Na (Fig. 5). The average K/Cl molar ratio of the fluid is 0.4 (range 0.07 to 0.71) and the (K+Na)/Cl ratio is 0.6 (range 0.22 to 1.88). The inclusion compositions fall along linear arrays from carbonate towards K–Na–Cl-rich compositions (Figs. 4 and 5), indicating the presence of a Cl-brine end-member. The calculated end-member carbonate and brine compositions are given in Table 3. The brine is similar to the composition of K–Cl-rich fluid in cloudy diamonds from Koffiefontein [4] and to the brine end-member fluid in a fibrous diamond from Diavik, Canada [6].

In most inclusions, the molar ratio Na+K/Cl is less than 1, therefore Cl in the inclusions is not fully charge balanced by the alkali cations. However, the sum of the charge associated with positive mono- and divalent (K, Na, Fe, Mg, Ca) ions is >100 (average 223) per 100 Cl ions and it is thought that the excess charge is balanced by carbonate ions as suggested by [4].

4.2.2. Eclogitic

Relative to the peridotitic fluid, the eclogitic fluid is Si- and Al-rich (Figs. 4 and 5). The high Si-content is consistent with the presence of quartz, which is observed in the infrared spectra. This chemical composition is similar to published data for fibrous diamonds from Zaire and Botswana [1,2], but the Panda fluid has a higher concentration of K, Cl and Ba. The eclogitic coat fluid is more Fe-rich (Mg#=0.2±0.1) than that in the peridotitic samples.

In fluid inclusions in the single eclogitic diamond, Cl is negatively correlated with Ca, Mg, Fe and Si, and positively correlated with K (Fig. 5). In consequence, the inclusion compositions fall along linear arrays from carbonate towards K–Cl-rich compositions (Fig. 4), again indicating the presence of a Cl-brine end-member. The average K/Cl molar ratio of the fluid is 0.45 (range 0.07 to 0.60). The calculated composition of the carbonate (low-Cl) and brine end-members is given in Table 3. The end-member brine composition in the eclogitic suite micro-inclusions is similar to that in the peridotitic diamond micro-inclusions except for its slightly higher Fe content.

5. Discussion

5.1. Mantle conditions during fibrous diamond growth

The compositions of the silicate inclusions in the Panda diamond coats indicate that fibrous diamonds can grow in both peridotitic and eclogitic host rocks. Therefore, fibrous diamonds grow in the same paragenetic environments as octahedral diamonds. The relatively low Mg# of garnet and olivine in the diamond coats are indicative of high source fertility. However the moderate to high Cr_2O_3 content of garnet and clinopyroxene suggests that the apparent fertility is due to a secondary process. Harzburgitic inclusions were not found in the Panda coats, this is in contrast to inclusions in octahedral diamonds from Panda, which are dominantly harzburgitic. Furthermore, the calculated *PT* conditions of the Panda coats place them within the ultra-depleted upper layer of the Slave lithosphere defined in [17,18]. The dominance of lherzolitic inclusions may suggest that the diamond coats formed during a localized re-fertilization event involving the influx of the co-existing Ca-rich fluid, which converted harzburgite to lherzolite. However, the absence of harzburgitic inclusions may be a sampling artifact.

Geothermometry of silicate macro-inclusions indicates that the Panda diamonds grew over a narrow temperature range of 930 to 1010 °C. These calculated temperatures from EDS analyses are lower than indicated by inclusions in non-fibrous diamonds from Panda (1100–1250 °C, [19]). For the amount of nitrogen present, the low degree of nitrogen aggregation is also

consistent with temperatures <1200 °C. Diamond growth at lower temperatures may be possible because of the high level of fluid supersaturation, which aids carbon diffusion at subsolidus mantle conditions. Synthetic diamonds grown in KCl [41] and carbonate–KCl [42] exhibit skeletal forms, testifying to high crystallisation rates in KCl-bearing systems. Geobarometry gives calculated equilibration pressures of 4.2–4.6 GPa for Panda coat inclusions.

The pressure–temperature conditions indicated by inclusion geothermobarometry of the lherzolitic Panda diamond coats fall just below the lherzolite+H_2O+CO_2 solidus of Wyllie et al., [43]. This is consistent with the presence of liquid water in all samples. These low temperatures also suggest that fibrous diamonds growth at Panda was not the result of a thermal event and favours a growth model driven by open system arrival of externally derived metasomatic fluids.

5.2. Origin of the silicate inclusions

The silicate inclusions in the Panda diamond coats are smaller and more abundant than silicate inclusions in octahedral diamonds. The silicate minerals in the diamond coats may be either: 1) syngenetic inclusions, which precipitated from the same fluid as the host diamond leaving a carbonate–KCl–H_2O-rich residual fluid; or 2) protogenetic inclusions from the mantle host in which diamond precipitated. Survival of the diamond cores is an important criterion for both of these models. These events are not thought to be late stages of core growth (i.e. from the residual melt) because the sharp boundary, and the difference in nitrogen aggregation states between the core and coat suggests that the two formed at separate times.

In the syngenetic scenario, the presence of both eclogitic and peridotitic silicate inclusions in the diamond coats indicates that fibrous diamond growth occurred during at least two events involving silicate-bearing melts, or during a single event straddling a paragenetic boundary. The small size and abundance of the silicate inclusions may reflect conditions in the growth environment: small and abundant minerals suggest that the nucleation rate was high. High levels of nucleation are generally attributed to supersaturation of the growth medium and/or to undercooling (growth temperature lower than saturation temperature). Silicate supersaturation of the fibrous diamond coat growth environment is considered unlikely because of the low Si-content of the trapped fluid and the low TiO_2 content of the garnet inclusions. The H_2O-rich nature of the coexisting fluid suggests that diffusion was likely to be fast, so the growth rate should not have limited the size of silicate crystals. However, the rapidly growing diamond host encapsulated the growing silicate inclusions and so may have limited their size. The low equilibration temperatures are consistent with undercooling, however rapid cooling is not considered likely in the upper mantle.

In the protogenetic scenario, the silicate macro-inclusions represent the host rocks (peridotitic and eclogitic) in which the diamond cores resided, and which have been modified by an incoming carbonate–H_2O metasomatic fluid similar to that trapped in the micro-inclusions. Significant melting of the silicate host rock did not occur in this scenario. This is consistent with the equilibration temperatures of the silicate inclusions, which are below the lherzolite+H_2O+CO_2 solidus. This is also consistent with the fact that the garnet and clinopyroxene inclusions have high Cr_2O_3, but fertile Mg# and CaO contents, suggesting that the apparent fertility is due to a secondary process. In this scenario, the small size of the silicate inclusions is due to preferential uptake of smaller crystals. This model is more consistent with the carbonate-rich, Si-poor nature of the trapped fluid.

A third scenario is that the host rock underwent subsolidus recrystallisation during passage of the fluid. In this case, the silicate inclusions are pre-existing and mainly represent the composition of the host rock (i.e. protogenetic), but grow together with the diamond (i.e. syngenetic). The small size of the silicate inclusions is due to the rapid growth of the fibrous diamond host which encases the recrystallising minerals, halting their growth. This model is consistent with the composition of garnet and clinopyroxene, with the growth of both eclogitic and peridotitic suite fibrous diamond during a single event and with the small size of the inclusions.

5.3. Nature of the trapped fluid

All the of the Panda diamond coat micro-inclusions contain H_2O and have carbonate and KCl in varying proportions. The similarity between the compositions of carbonate in the peridotitic and eclogitic samples suggests that this fluid may have been derived externally and percolated through both paragenetic environments. In this scenario, the peridotitic and eclogitic diamond coats grew in the same metasomatic event.

Klein-BenDavid et al. [6], suggest that the carbonatite melt evolves towards a more KCl-rich composition by mineral crystallisation. During late stage crystallisation, the residual melt/fluid will contain a higher concentration of KCl and Ba. This mechanism may explain the small scale variations in observed micro-

inclusion compositions. Olivine and clinopyroxene found in the some of the fluid micro-inclusions may be precipitates from such a carbonatite melt.

The carbonate-, KCl- and H_2O-rich fluid inclusions represent the residual fluid after precipitation of diamond. The prevailing oxidation state during fluid influx and diamond coat formation is constrained by the need for diamond to remain stable throughout, so that the diamond cores are preserved. The upper limit of diamond stability in lherzolite is defined by the reaction: enstatite + magnesite = forsterite + diopside + diamond (EMODD), which occurs approximately −1.5 log fO_2 below the fayalite–magnetite–quartz buffer [44]. Diamond and carbonate may co-exist at this reaction line. The diamond coat may have formed from the parental C-bearing fluid, either by reduction of an oxidized fluid, such as CO_2 (where the wall rock has been armored from carbonate forming reactions) and carbonate or by the oxidation of a reduced fluid, such as CH_4:1) If the initial fluid was reducing, then oxidation would drive the fluid composition to higher fO_2. The fluid would initially precipitate diamond and carbonate would only form once the EMODD buffer was intersected. However, CH_4 is not detected in the FTIR spectra of the diamond coats and carbonate is not concentrated towards the rim of the diamond coats. Furthermore, in this scenario, carbonate is formed at the expense of diamond. 2) If the initial fluid was oxidising, then the fO_2 of the fluid must have been lowered by reaction with the more reducing host mantle. Once the fluid intersected the EMODD buffer, diamond would have been precipitated at the expense of carbonate. The reduction process was buffered by the formation of diamond, this allowed carbonate to coexist with diamond throughout the growth of the coat. The redox state of the host mantle is raised slightly during interaction with the incoming fluid, but do not increase above the EMODD buffer, therefore the diamond cores remain stable throughout. The similarity between the composition of the carbonate components in the peridotitic and eclogitic samples also support the suggestion that the incoming fluid was carbonate-rich, rather than reducing. Therefore, we suggest that this fluid was then reduced by interaction with the minerals of the host rock to form the fibrous diamond coats. Mössbauer analysis of spinel and garnet in mantle xenoliths from the Slave craton indicate that the lithosphere is quite reduced [45] and hence capable of reducing carbonate to diamond.

The Si-rich fluid component, which is virtually absent in the peridotitic samples, is an important component of the fluid in the single eclogite sample. This is emphasized by the presence of quartz in the inclusions. This suggests that this silicate end-member fluid component may have been derived locally. The high Si-content of the eclogite fluid relative to the peridotite fluid may be due to either: 1) metasomatic interaction between the fluid and host rock as a result of the fact that eclogite is typically Si-saturated. On the one hand the Si-content of the eclogitic fluid may be increased by metasomatic reactions between the fluid and Si- and Al-rich minerals present in eclogite. On the other hand, the Si-content of the peridotitic fluid may be reduced by reactions to convert olivine to orthopyroxene, as a result of the low Si-activity of peridotite. 2) Partial melting of the eclogite host rock as a result of the lower temperature of the eclogite + H_2O solidus [46]. In both these scenarios, the silicate signature is generated locally. SiO_2 is thought to have crystallized from the trapped silicate fluid component.

5.4. Relationship between the diamond core and its coat

For the purposes of this section, we assume that the Panda diamond cores are part of the same diamond population as normal octahedral diamonds sampled by the Panda kimberlite. The similarity between the nitrogen content and degree of nitrogen aggregation in the diamond cores in this study and of undeformed octahedral diamonds from Panda [19,47] suggests that the populations may be broadly contemporaneous.

The contrasting nitrogen characteristic of the diamond core and its coat suggests that they grew during separate events. This is supported by the sharp boundary between the core and coat in the CL image. Nitrogen in the cores is more aggregated (up to ~ 30% IaB centres) than in the coat (100% IaA), suggesting that the growth of the coat was succeeded by a period of mantle residence prior to the growth of the coat. Growth during separate events is supported by the lower equilibration temperature of the coat inclusions, relative to those in Panda octahedral diamonds [19]. Therefore we assume that the growth of the diamond cores, which are equivalent to normal octahedral diamonds, occurred some time before the growth of their fibrous coats, and that the host mantle cooled by approximately 200 °C in the intervening period. If the macro inclusions are indeed protogenetic, then the diamond coat inclusions come from the same host rocks as those in octahedral diamonds from Panda [19,20], so may be directly compared.

The coat inclusions extend the compositional range of Panda diamond inclusion compositions from relatively undepleted inclusions in octahedral diamonds [19,20] to more fertile Fe- and Ca-rich compositions (lower Mg# and higher Ca#). When

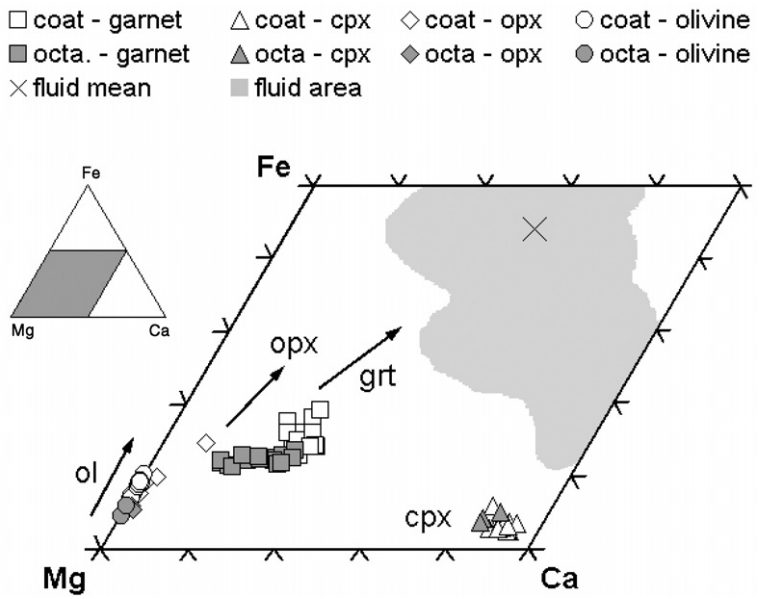

Fig. 6. Ternary diagram showing the compositions of garnet (squares), olivine (circles), orthopyroxene (diamonds) and clinopyroxene (triangles) inclusions in octahedral (octa.) diamonds (grey-filled symbols) [19,20] and the fibrous diamond coats (open symbols) and of the average fluid composition (cross) and field of measured fluid compositions (grey filled area) in micro-inclusions in the coat. Garnet, opx and olivine in the diamond coat trend away from the composition of equivalent minerals in octahedral diamond in the direction of the trapped fluid composition.

compared to the composition of the trapped fluid (Fig. 6), it can be seen that the compositions of garnet, olivine and orthopyroxene inclusions in the Panda diamond coats are more Fe-rich, and garnet and orthopyroxene are more Ca-rich than equivalent minerals in octahedral Panda diamonds. The trend between the compositions of octahedral and coat inclusion compositions is towards the composition of the Fe- and Ca-rich carbonate observed in the coat micro-inclusions. This suggests that the inclusions in the diamond coats may be protogenetic and that the primary compositions have been altered by metasomatic interaction with the fluid, or that the primary minerals underwent subsolidus recrystallisation in the presence of the fluid. Therefore, the differences between octahedral diamond and diamond coat inclusion compositions may provide a snap-shot of mantle metasomatism. A remnant of the primary mineral compositions is preserved in the moderate to high Cr_2O_3 contents of garnet and clinopyroxene and the Ni content of olivine. The metasomatic event was probably localised, for example to vein walls, firstly because H_2O-rich fluids have high dihedral angles in mantle rocks: ~ 40° in dunite [48] and higher in multi-mineralic peridotites; and >60° in eclogite [49] at 5 GPa. The diamond-forming H_2O-rich fluids can thus only infiltrate grain edges under conditions of high fluid volume or host-rock deformation.

6. Conclusions

Panda diamond coats contain macro-inclusions of olivine, garnet, orthopyroxene and clinopyroxene. Both peridotitic (lherzolitic) and eclogitic suite minerals are represented, therefore fibrous diamonds may grow in the same paragenetic environments as octahedral diamonds. The calculated equilibration temperatures for the peridotitic coat inclusions (930 to 1010 °C) are lower than indicated by inclusions in octahedral diamonds from Panda (1100–1250 °C; [19]) and fall below the lherzolite+H_2O+CO_2 solidus [39]. The silicate inclusions have low values of Mg# and have higher Ca# values than equivalent minerals in octahedral diamonds from Panda [19,20]. The coat inclusion compositions trend away from those of equivalent phases in octahedral diamonds from Panda in the direction of the trapped fluid. This suggests that the chemical differences between inclusions in octahedral diamonds and those in the diamond coats record the effect of mantle metasomatism.

The co-existing fluid micro-inclusions are dominated by H_2O, carbonate and KCl. Fluid inclusions lie along linear arrays between Fe–Ca–Mg carbonate and KCl. Inclusions in the peridotitic samples contain very low or zero concentrations of Si–Al and do not contain quartz. In contrast, the eclogitic sample has quartz in its infrared spectra and its inclusions do contain moderate concentrations of Si and Al. We suggest that the carbonate–

H_2O–KCl fluid component may have been externally derived, possibly from a subducted slab, and percolated through both peridotitic and eclogitic diamond (core) bearing mantle. Metasomatism of the host mantle modified the fluid composition. Diamond precipitated from this fluid, and the micro-inclusions represent the residue after metasomatism and mineral (including diamond) precipitation.

Acknowledgements

This work is funded by and EPSRC (award no. 01302499) industrial CASE studentship with DeBeers. Andy Taylor and Jacques Jones (DTC research, Maidenhead) are thanked for laser cutting and sample preparation. Thomas Stachel, Andy Beard and an anonymous reviewer are thanked for valuable feedback in review.

Appendix A. Supplementary Data

Supplementary data associated with this article can be found in the online version, at doi:10.1016/j.epsl.2006.08.005.

References

[1] O. Navon, I.D. Hutcheon, G.R. Rossman, G.J. Wasserburg, Mantle-derived fluids in diamond micro-inclusions, Nature 335 (1988) 784–789.
[2] M. Schrauder, O. Navon, Hydrous and carbonatitic mantle fluids in fibrous diamonds from Jwaneng, Botswana, Geochim. Cosmochim. Acta 58 (2) (1994) 761–771.
[3] M. Schrauder, C. Koeberl, O. Navon, Trace element analyses of fluid-bearing diamonds from Jwaneng, Botswana, Geochim. Cosmochim. Acta 60 (23) (1996) 4711–4724.
[4] E.S. Izraeli, J.W. Harris, O. Navon, Brine inclusions in diamonds: a new upper mantle fluid, Earth Planet. Sci. Lett. 187 (3–4) (2001) 323–332.
[5] E.S. Izraeli, J.W. Harris, O. Navon, Fluid and mineral inclusions in cloudy diamonds from Koffiefontein, South Africa, Geochim. Cosmochim. Acta 68 (11) (2004) 2561–2575.
[6] O. Klein-BenDavid, E.S. Izraeli, E. Hauri, O. Navon, Mantle fluid evolution — a tale of one diamond, Lithos 77 (1–4) (2004) 243–253.
[7] H.O.A. Meyer, Inclusions in diamond, in: P.H. Nixon (Ed.), Mantle Xenoliths, Wiley-Interscience, 1987, pp. 501–522.
[8] J.W. Harris, Diamond geology, in: J.E. Field (Ed.), The Properties of Natural and Synthetic Diamonds, Academic Press, Oxford, UK, 1992, pp. 384–385.
[9] T. Stachel, Diamonds from the asthenosphere and the transition zone, Eur. J. Mineral. 13 (5) (2001) 883–892.
[10] Y. Kamiya, A.R. Lang, On the structure of coated diamonds, Philos. Mag. 11 (1965) 347–357.
[11] G.D. Guthrie, D.R. Veblen, O. Navon, G.R. Rossman, Submicrometer fluid inclusions in turbid-diamond coats, Earth Planet. Sci. Lett. 105 (1–3) (1991) 1–12.
[12] A.R. Lang, J.C. Walmsley, Apatite inclusions in natural diamond coat, Phys. Chem. Miner. 9 (1) (1983) 6–8.
[13] J.C. Walmsley, A.R. Lang, Oriented biotite inclusions in diamond coat, Mineral. Mag. 56 (382) (1992) 108–111.
[14] J.C. Walmsley, A.R. Lang, On sub-micrometer inclusions in diamond coat — crystallography and composition of ankerites and related rhombohedral carbonates, Mineral. Mag. 56 (385) (1992) 533–543.
[15] R.A. Creaser, H. Grutter, J. Carlson, B. Crawford, Macrocrystal phlogopite Rb–Sr dates for the Ekati property kimberlites, Slave Province, Canada: evidence for multiple intrusive episodes in the Paleocene and Eocene, Lithos 76 (1–4) (2004) 399–414.
[16] T. Nowicki, B. Crawford, D. Dyck, J. Carlson, R. McElroy, P. Oshust, H. Helmstaedt, The geology of kimberlite pipes of the Ekati property, Northwest Territories, Canada, Lithos 76 (1–4) (2004) 1–27.
[17] A. Menzies, K. Westerlund, H. Grutter, J. Gurney, J. Carlson, A. Fung, T. Nowicki, Peridotitic mantle xenoliths from kimberlites on the Ekati Diamond Mine property, NWT, Canada: major element compositions and implications for the lithosphere beneath the central Slave craton, Lithos 77 (1–4) (2004) 395–412.
[18] W.L. Griffin, B.J. Doyle, C.G. Ryan, N.J. Pearson, S.Y. O'Reilly, R. Davies, K. Kivi, E. Van Achterbergh, L.M. Natapov, Layered mantle lithosphere in the Lac de Gras area, Slave Craton: composition, structure and origin, J. Petrol. 40 (5) (1999) 705–727.
[19] R. Tappert, T. Stachel, J.W. Harris, N. Shimizu, G.P. Brey, Mineral inclusions in diamonds from the Panda kimberlite, Slave Province, Canada, Eur. J. Mineral. 17 (3) (2005) 423–440.
[20] T. Stachel, J.W. Harris, R. Tappert, G.P. Brey, Peridotitic diamonds from the Slave and the Kaapvaal cratons — similarities and differences based on a preliminary data set, Lithos 71 (2–4) (2003) 489–503.
[21] K.J. Westerlund, S.H. Shirley, S.H. Richardson, J.J. Gurney, J.W. Harris, Re–Os systematics of diamond inclusion sulfides from the Panda kimberlite, Slave Craton, Extended Abstracts of the 8th International Kimberlite Conference, FLA_0134, Victoria, Canada, 2003.
[22] M.J. Mendelssohn, H.J. Milledge, Geologically significant information from routine analysis of the mid-infrared spectra of diamonds, Int. Geol. Rev. 37 (1995) 95–110.
[23] S.R. Boyd, D.P. Mattey, C.T. Pillinger, H.J. Milledge, M.J. Mendelssohn, M. Seal, Multiple growth events during diamond genesis: an integrated study of carbon and nitrogen isotopes and nitrogen aggregation state in coated stones, Earth Planet. Sci. Lett. 86 (2–4) (1987) 341–353.
[24] S.R. Boyd, C.T. Pillinger, H.J. Milledge, M.J. Seal, C-isotopic and N-isotopic composition and the infrared-absorption spectra of coated diamonds — evidence for the regional uniformity of CO_2–H_2O rich fluids in lithospheric mantle, Earth Planet. Sci. Lett. 108 (1–3) (1992) 139–150.
[25] S.R. Boyd, F. Pineau, M. Javoy, Modeling the growth of natural diamonds, Chem. Geol. 116 (1–2) (1994) 29–42.
[26] W.K. Thompson, Infra-red spectroscopic studies of aqueous systems. Part 1. Molar extinction coefficients of water, deuterium oxide, deuterium hydrogen oxide, aqueous sodium chloride and carbon disulphide, Transactions of the Faraday Society, vol. 61, 1965, pp. 2635–2640.
[27] G. Fine, E. Stolper, The speciation of carbon-dioxide in sodium aluminosilicate glasses, Contrib. Mineral. Petrol. 91 (2) (1985) 105–121.

[28] H.S. O'Neill, B.J. Wood, An experimental study of FeMg partitioning between garnet and olivine and its calibration as a geothermometer, Contrib. Mineral. Petrol. 70 (1978) 59–70.
[29] J.J. Gurney, B. Harte, K.G. Cox, Mantle xenoliths in the Matsoku kimberlite pipe, Phys. Chem. Earth 9 (1975) 507–529.
[30] M. Matthews, B. Harte, D. Prior, Mantle garnets — a cracking yarn, Geochim. Cosmochim. Acta 56 (7) (1992) 2633–2642.
[31] L.L. Perchuk, O.G. Safonov, V.O. Yapaskurt, J.M. Barton, Crystal–melt equilibria involving potassium-bearing clinopyroxene as indicator of mantle-derived ultrahigh-potassic liquids: an analytical review, Lithos 60 (3–4) (2002) 89–111.
[32] H.S. O'Neill, An experimental study of FeMg partitioning between garnet and olivine and its calibration as a geothermometer: corrections, Contrib. Mineral. Petrol. 72 (1980) 337.
[33] E.J. Krogh, The garnet–clinopyroxene Fe–Mg geothermometer — a reinterpretation of existing experimental-data, Contrib. Mineral. Petrol. 99 (1) (1988) 44–48.
[34] P. Nimis, W.R. Taylor, Single clinopyroxene thermobarometry for garnet peridotites. Part I. Calibration and testing of a Cr-in-Cpx barometer and an enstatite-in-Cpx thermometer, Contrib. Mineral. Petrol. 139 (5) (2000) 541–554.
[35] H.N. Pollack, D.S. Chapman, On the regional variation of heat flow, geotherms, and lithospheric thickness, Tectonophysics 38 (1977) 279–296.
[36] F.R. Boyd, J.J. Gurney, Diamonds and the African lithosphere, Science 232 (1986) 472–477.
[37] W.L. Griffin, J.J. Gurney, C.G. Ryan, Variations in trapping temperatures and trace elements in peridotite-suite inclusions from African diamonds — evidence for two inclusion suites, and implications for lithosphere stratigraphy, Contrib. Mineral. Petrol. 110 (1992) 1–15.
[38] T. Stachel, J.W. Harris, Syngenetic inclusions in diamond from the Birim field (Ghana) — a deep peridotitic profile with a history of depletion and re-enrichment, Contrib. Mineral. Petrol. 127 (4) (1997) 336–352.
[39] P.J. Wyllie, Experimental petrology of upper-mantle materials, process and products, J. Geodyn. 20 (4) (1995) 429–468.
[40] White, The carbonate minerals, in: V.C. Farmer (Ed.), The Infrared Spectra of Minerals, Mineralogical Society, London, 1974, pp. 227–284.
[41] Y.A. Litvin, Alkaline-chloride components in processes of diamond growth in the mantle and high-pressure experimental conditions, Dokl. Earth Sci. 389 (3) (2003) 388–391.
[42] E. Tomlinson, A. Jones, J. Milledge, High-pressure experimental growth of diamond using C–K_2CO_3–KCl as an analogue for Cl-bearing carbonate fluid, Lithos 77 (1–4) (2004) 287–294.
[43] P.J. Wyllie, I.D. Ryabchikov, Volatile components, magmas, and critical fluids in upwelling mantle, J. Petrol. 41 (7) (2000) 1195–1206.
[44] R.W. Luth, Diamonds, eclogites, and the oxidation-state of the Earth's mantle, Science 261 (5117) (1993) 66–68.
[45] C.A. McCammon, M.G. Kopylova, A redox profile of the Slave mantle and oxygen fugacity control in the cratonic mantle, Contrib. Mineral. Petrol. 148 (1) (2004) 55–68.
[46] D. Vielzeuf, M.W. Schmidt, Melting relations in hydrous systems revisited: application to metapelites, metagreywackes and metabasalts, Contrib. Mineral. Petrol. 141 (3) (2001) 251–267.
[47] K.J. Westerlund, J.J. Gurney, R.W. Carlson, S.B. Shirey, E.H. Hauri, S.H. Richardson, A metasomatic origin for Late Archean eclogitic diamonds: implications from internal morphology of diamonds and Re–Os and S isotope characteristics of their sulfide inclusions from the Late Jurassic Klipspringer kimberlites, S. Afr. J. Geol. 107 (1–2) (2004) 119–130.
[48] K. Mibe, T. Fujii, A. Yasuda, Connectivity of aqueous fluid in the Earth's upper mantle, vol. 25 (8), 1998, pp. 1233–1236.
[49] K. Mibe, T. Yoshino, S. Ono, A. Yasuda, T. Fujii, Connectivity of aqueous fluid in eclogite and its implications for fluid migration in the Earth's interior, J. Geophy. Res.–Solid Earth 108 (B6) (2003) art. no.—2295.
[50] R. Berman, R. Simon, On the graphite–diamond equilibrium, Zeit. Elektrochem. 59 (1955) 333–338.